ACS Macro Letters

Letter

pubs.acs.org/macroletters

Synthesis and Stereocomplex Crystallization of Poly(lactide)–Graphene Oxide Nanocomposites

Yang Sun[†] and Chaobin He*[,†,‡]

[†]Department of Materials Science & Engineering, National University of Singapore, 9 Engineering Drive 1, 117576 Singapore

[‡]Institute of Materials Research and Engineering, Agency for Science, Technology and Research (A*STAR), 3 Research Link, 117602 Singapore

ABSTRACT: Poly(lactide) (PLA)–graphene oxide (GO) nanocomposites were prepared by blending commercial poly(L-lactide) (PLLA) with GO-g-PDLA, where GO-g-PDLA was synthesized via ring-opening polymerization using modified GO as the initiator. Fourier transform infrared spectroscopy (FT-IR), differential scanning calorimetry (DSC), and X-ray diffraction (XRD) studies showed that a stereocomplex crystal could be formed between PLLA and GO-g-PDLA. The incorporation of GO nanofillers leads to a lower crystallization activation energy of stereocomplex and a higher crystallinity in solution casting samples, mainly due to the heterogeneous nucleating effect of the well-dispersed covalently bonded GO sheets, while in cold crystallized samples, the crystallinity was low owing to exfoliated GO sheets which may reduce chain mobility and hinder crystal growth.

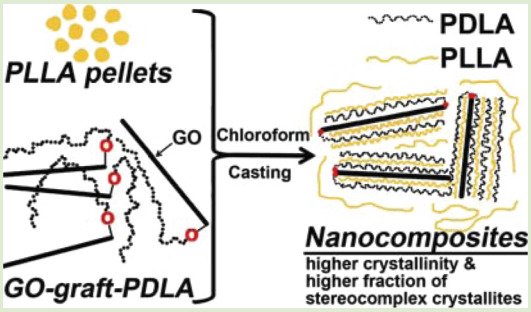

Poly(lactide) (PLA) is a plant-derived biodegradable polymer that is widely used as an alternative to petroleum-derived polymers.[1] It has three isomeric forms, that is, poly(L-lactide) (PLLA), poly(D-lactide) (PDLA), and poly(racemic-lactide) (PDLLA), which display a wide variety of properties. Stereocomplexation can occur between PLLA and PDLA either in solution or in a solid state from the melt,[2] which results in the formation of a stereocomplex crystallite (sc-crystallite) different from the homocrystallite PLLA or PDLA.[3] The sc-crystallite has been extensively studied,[1,3−5] and it gives PLA-based materials higher mechanical performances, thermal resistance, and hydrolysis resistance, thus opening a new way to produce various types of biodegradable materials.[2] Our previous study using molecular modeling also found that better thermal and mechanical properties observed in the PLA stereocomplex could be attributed to the formation of an extra hydrogen bond in the sc-crystallite.[6]

Graphene is a one-atom-thick planar sheet of sp^2-bonded carbon atoms in a densely packed honeycomb crystal lattice.[7] In recent years, polymer/graphene nanocomposites have attracted much attention due to their outstanding electrical, optical, electrochemical, and mechanical properties,[8−10] and one of the prerequisites for achieving the desired reinforcing effect is the homogeneous incorporation of graphene sheets in various matrices and a strong matrix/graphene interaction. However, the intrinsic $\pi-\pi$ stacking interaction between graphene layers easily results in agglomeration, and the interaction between the graphene sheet and the polymer matrix is dominated by van der Waals interactions.[11] On the other hand, graphene oxide (GO), a surface modified version of graphene with functional groups, for example, −OH, −O− on the basal plane, and −COOH at the edges,[12] could achieve a much enhanced dispersion in polar matrices.

Graphene and GO have been utilized in PLLA nanocomposites.[13−17] It is found that expanded graphite or GO can increase the crystallinity of the nanocomposite.[14,16] In this letter, we report a new type of PLA-GO nanocomposite formed through stereocomplexation. First, GO was modified by grafting PDLA to form GO-g-PDLA, for which similar protocols have been reported.[18,19] Then the resulting GO-g-PDLA was blended with commercial PLLA to form PLA-GO nanocomposites. The covalent combination of GO and PDLA could be expected as both a promising heterogeneous nucleating agent and a reinforcing filler for PLLA-based materials. Furthermore, the formation of stereocomplex between PLLA and PDLA on GO could ensure a strong filler–matrix interaction. There is however no literature report on the PLA-GO nanocomposite formed by the stereocomplex of PLLA and GO-g-PDLA so far.

The GO-g-PDLA was synthesized by ring-opening polymerization of D-lactide monomers, initiated by the grafted OH groups on GO and under the catalysis of $Sn(Oct)_2$ as shown in Scheme 1. The GO-g-PDLA was later blended with commercial PLLA in chloroform to form the stereocomplex nanocomposite (see the Experimental Section). As GO sheets are covalently bonded to PDLA chains, the possibility of GO agglomeration is very low, and a good GO dispersion has been achieved as shown in Figure 1. The solution casting nanocomposites show

Received: March 19, 2012
Accepted: May 14, 2012
Published: May 22, 2012

   dx.doi.org/10.1021/mz300131u | *ACS Macro Lett.* 2012, 1, 709−713

Scheme 1. Synthesis of GO-g-PDLA

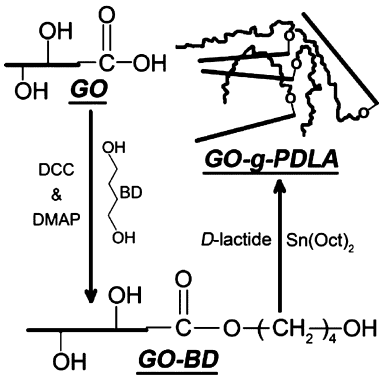

improved crystallinity and a higher fraction of sc-crystallites brought about by the GO sheets.

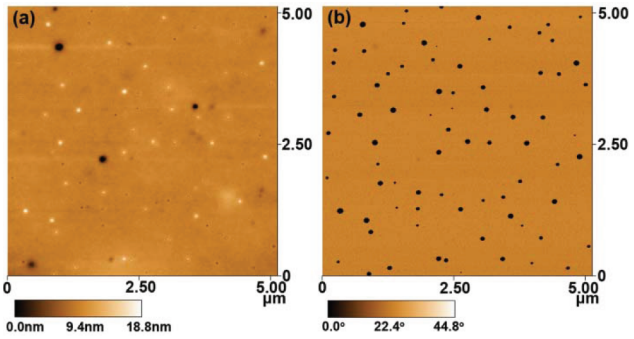

Figure 1. AFM images of a solution casting nanocomposite film with 30 wt % of PLLA and 70 wt % of GO-g-PDLA: (a) height, (b) phase.

Fourier transform infrared (FT-IR) spectra confirmed the successful modification of GO as shown in Figure 2a. The IR absorption at 1729 cm^{-1} for GO-g-1,4-butanediol (GO-BD) is

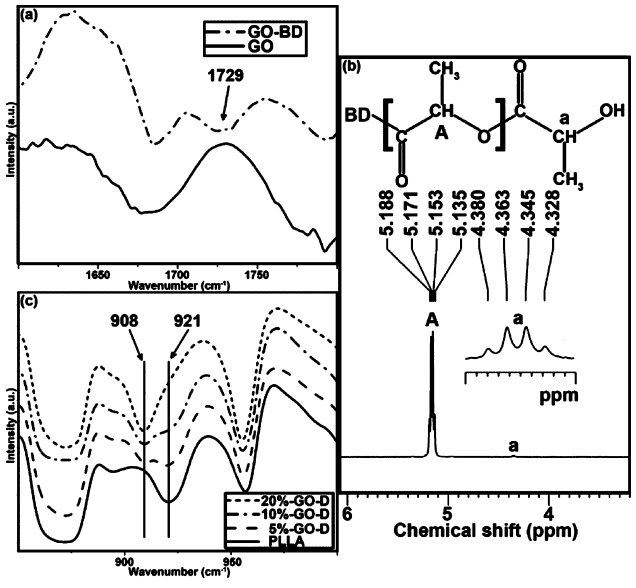

Figure 2. (a) FT-IR spectra of neat GO and GO-BD in the range 1600−1800 cm^{-1}. (b) ^1H NMR spectrum of GO-g-PDLA. (c) FT-IR spectra of stereocomplex nanocomposites of PLLA with GO-g-PDLA in the range 850−1000 cm^{-1}.

assigned to the C═O stretching vibration of ester groups between GO and BD. ^1H NMR spectrum was used to measure the molecular weight of GO-g-PDLA as shown in Figure 2b. The peaks labeled as "A" at around 5.16 ppm are ascribed to methine protons −CH−, while "a" at around 4.35 ppm corresponds to the methine group −CH− located at the end of PDLA chain which is adjacent to the terminal hydroxyl groups.[19] According to the ^1H NMR spectrum, using the relative intensities of "A" and "a", the number average molecular weight (M_n) of the PDLA chains grafted on GO is calculated to be 9360. As a comparison, the neat linear PDLA used for the control samples has a similar M_n, that is, 12 000.

To study the formation of sc-crystallites in the resulting nanocomposite films, FT-IR spectra were employed, as shown in Figure 2c. The IR absorptions at 921 cm^{-1} and 908 cm^{-1} are ascribed to the homocrystallites and sc-crystallites, respectively.[3] With increasing GO-g-PDLA contents, the 921 cm^{-1} band (PLLA) is gradually weakened while the 908 cm^{-1} band (20%-GO-D) becomes predominant, which provides clear evidence of sc-crystallite formation between GO-g-PDLA and PLLA.

Further confirmation of stereocomplex between PLLA matrix and GO-g-PDLA comes from the differential scanning calorimetry (DSC) study as shown in Figure 3a, in which

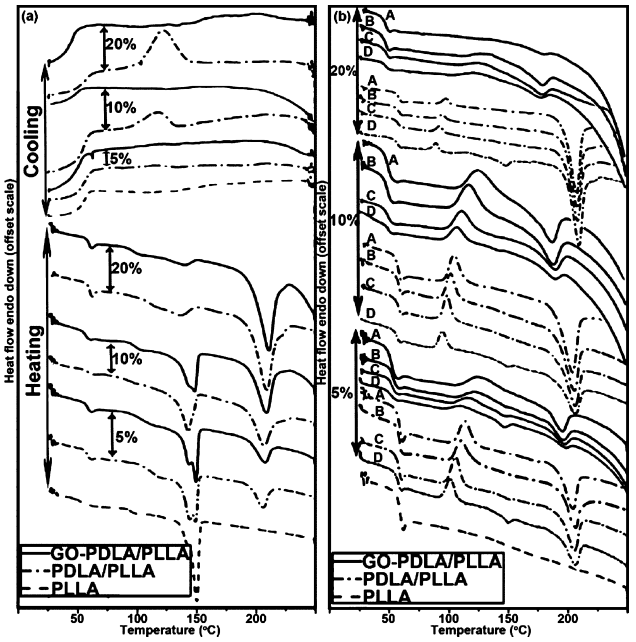

Figure 3. Differential scanning calorimetry (DSC) thermograms of PLLA, the stereocomplex nanocomposites, and the control samples: (a) first heating and cooling scans (all at 10 °C/min) of the solution casting samples. (b) The heating scans (PLLA at 10 °C/min, and A: 10 °C/min, B: 7 °C/min, C: 5 °C/min, D: 3 °C/min) of the melt-cooled samples obtained in a.

PLLA exhibits only one melting peak at around 150 °C at the first heating scan, corresponding to the homocrystallites, while the stereocomplex nanocomposites show an additional melting peak at around 210 °C at the first heating scan, indicating the formation of sc-crystallites for solution casting GO-g-PDLA/PLLA nanocomposites. DSC thermograms of the control samples consisting of stereocomplex of neat linear PDLA and PLLA were also shown in Figure 3a as a comparison, where we could also see the existence of a melting peak at around 210 °C.

dx.doi.org/10.1021/mz300131u | ACS Macro Lett. 2012, 1, 709−713

Using the peak temperatures of cold crystallization at different heating rates as shown in Figure 3b, the crystallization activation energy E_{av} for the stereocomplex nanocomposites with different GO-g-PDLA loadings and the corresponding control samples (linear PDLA blended with PLLA) could be calculated as tabulated in Table 1. It is found that, with an increase of GO concentration, the activation energy, E_{av}, for the stereocomplex nanocomposites was first reduced from 22.8 kcal/mol for 5 wt % of GO-g-PDLA/PLLA to 16.9 kcal/mol for 10 wt % of GO-g-PDLA/PLLA and then increased to 25.6 kcal/mol for 20 wt % of GO-g-PDLA/PLLA. It is estimated that the effective GO concentration for the 20 wt % GO-g-PDLA/PLLA system is about 0.1 wt %. The reduction of activation energy could be attributed to the heterogeneous nucleating effect of the well-dispersed covalently bonded GO sheets. The latter increase of activation energy could be associated with the confinement of polymer chains when the GO concentration is too high, as the two-dimensional GO "divides" PLLA matrix into many different small "compartments", which reduces the transportation ability of polymer chains.

Table 1. DSC and WAXD Characterization Data of PLLA, the Stereocomplex Nanocomposites, and the Control Samples

	DSC	WAXD		
	activation energy[a]	crystallinity[b] (%)		
sample	E_{av} (kcal/mol)	casting	cold crystallized	sc/α fraction ratio of casting samples[c]
5%-D	24.2	39.74 ± 2.38	8.03 ± 0.61	0.53
5%-GO-D	22.8	50.38 ± 4.70	7.63 ± 0.79	0.68
10%-D	32.0	51.39 ± 2.62	15.71 ± 0.68	0.71
10%-GO-D	16.9	57.17 ± 2.24	11.85 ± 0.95	1.15
20%-D	38.9	60.64 ± 2.35	33.12 ± 0.41	0.52
20%-GO-D	25.6	68.88 ± 2.65	7.66 ± 0.99	2.79
PLLA		41.38 ± 2.00		

[a] E_{av} is calculated using the DSC heating scans in Figure 3b according to Kissinger's method; that is, $E_{av} = d\ln[\beta/T_p^2]/d[1/T_p] \times (-R)$, where β is the heating rate in K·min^{-1}, T_p is the maximum temperature of the cold crystallization peak in K, and R is the gas constant in kcal/(mol·K). [b] The crystallinity is calculated by crystallinity = $A_c/(A_c + A_a)$, where A_c and A_a are the areas of crystal peaks and amorphous peaks, respectively, in the wide area X-ray diffraction (WAXD) diffractograms. [c] This ratio is the area ratio of sc peaks (11.9°, 20.7°, and 23.9°) and α peaks (14.7°, 16.6°, 19.1°, and 22.2°).

Compared with the control samples in which the stereocomplex is formed between neat linear PDLA and PLLA without GO, the corresponding GO-g-PDLA/PLLA stereocomplex nanocomposites have substantially lowered E_{av}, especially at high loadings of GO-g-PDLA (10 wt % and 20 wt %). This further confirms the conspicuous heterogeneous nucleating effect of the well-dispersed covalently bonded GO sheets. As for PLLA, there is no crystal formation on the first DSC cooling curve neither on the second DSC heating curve, indicating the slow crystallization behavior of the polymers. This, on the other hand, demonstrates the usefulness of exploiting stereocomplexation to enhance the crystallinity and hence the thermal mechanical property of PLA.

The effect of GO and stereocomplexation on the crystallization of PLA was further investigated by wide-angle X-ray diffraction (WAXD). For the as-prepared solution casting samples as shown in Figure 4a, PLLA exhibits diffraction peaks at 2θ = 14.7°, 16.6°, 19.1°, and 22.2°, corresponding to the α-form homocrystallites,[20] while the stereocomplex nanocomposites and control samples exhibit additional peaks at 2θ = 11.9°, 20.7°, and 23.9°, corresponding to the sc-crystallites.[21] It is shown that all of the GO-g-PDLA/PLLA nanocomposites have a higher crystallinity than their corresponding control counterparts (Table 1). Moreover, the fraction of sc-crystallites in the solution casting samples is also greatly enhanced by GO sheet incorporation and increases with GO contents. These improvements are quite significant considering that only a small amount of GO (the GO concentration in 20 wt % GO-g-PDLA/PLLA is ~0.1 wt %) exists in the nanocomposites.

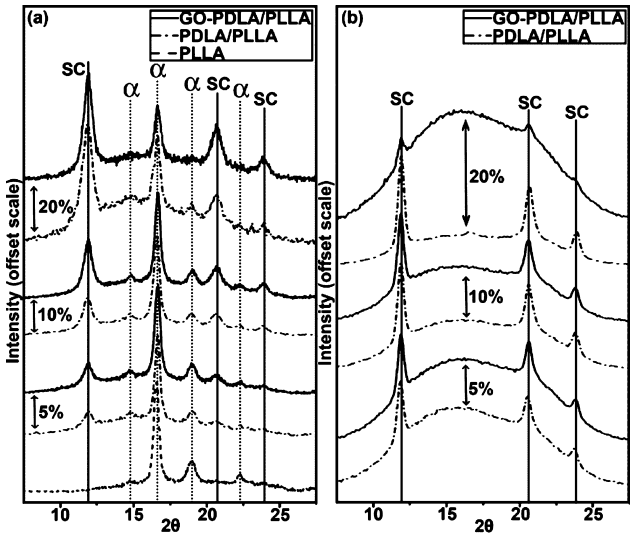

Figure 4. WAXD diffractograms of (a) the solution casting samples and (b) the cold crystallized samples.

It is worth mentioning, however, that the crystallization behavior of stereocomplex nanocomposites in condense states (melt or solid) is quite different from that in solution casting processes. Looking at the first DSC cooling scans in Figure 3a, we can see that there is a crystallization exothermal peak for the control samples, yet almost no crystallization happens during the cooling process for the stereocomplex nanocomposites. In the second DSC heating scans as shown in Figure 3b, cold crystallization takes place at a higher temperature for the stereocomplex nanocomposites compared to the corresponding control samples. In addition, the cold crystallization and melting peaks of the stereocomplex nanocomposites are broader than the corresponding control samples. These phenomena demonstrate that GO sheets impair the crystallization of stereocomplex nanocomposites in condense states. Furthermore, WAXD diffractograms of the cold crystallized samples only exhibit characteristic peaks of sc-crystallites as shown in Figure 4b. During cold crystallization, the stereocomplex nanocomposites have lower crystallinities than the control samples (Table 1), which further confirms GO's impairing role in the solid-state crystallization.

To understand the effect of GO on crystallization behavior of the stereocomplex nanocomposites, two key mechanisms need to be taken into consideration. The first is the activation energy

dx.doi.org/10.1021/mz300131u | ACS Macro Lett. 2012, 1, 709−713

for crystallization. GO can act as efficient heterogeneous nucleating sites and therefore lower the crystallization activation energy, as shown by DSC study. The second is that when the GO concentration is sufficiently high, it can inversely act as blocking sites, which hinders the growth of polymer crystallites due to limited polymer chain mobility.

In the solution casting process, as the solution is quite dilute, polymer chain mobility is high, which offers a relatively favorable environment for the growth of polymer crystallites. In this case, the lowered E_{av} resulting from GO's heterogeneous nucleating effect contributes predominantly, thus improving the crystallinity of stereocomplex nanocomposites and enhancing the fraction of sc-crystallites.

In condense states, the homogeneous and dense distribution of two-dimensional GO sheets in the PLA matrix may result in lower polymer chain mobility. Although E_{av} is lower in the stereocomplex nanocomposites and more crystallization processes may be initiated on GO substrates, the growth of polymer crystallites are hindered by neighboring GO sheets or crystallites, which hence leads to a low crystallinity. The "confinement" effect is also confirmed in DSC studies in Figure 3b, where the melting temperatures of the cold crystallized stereocomplex nanocomposite samples are lower than the corresponding control counterparts, indicating smaller crystalline sizes possibly resulting from the "confinement" effect and low polymer chain mobility.

To summarize, PLA-GO nanocomposites were successfully prepared by blending of commercial PLLA with GO-g-PDLA, where GO-g-PDLA was synthesized via ring-opening polymerization using modified GO as an initiator. The formation of a stereocomplex between GO-g-PDLA and PLLA matrix was evident by FT-IR, DSC, and WAXS studies. For the solution casting samples, the incorporation of GO nanofillers leads to a lower crystallization activation energy, an enhanced crystallinity, and a higher fraction of sc-crystallites compared with a neat linear PDLA/PLLA stereocomplex system. This could be attributed to the heterogeneous nucleating effect of GO. On the other hand in condense states, although GO could lower the activation energy of sc-crystallization, the confinement effect of two-dimensional GO and the resulting low polymer chain mobility lead to lower crystallinity and smaller crystalline sizes observed in the stereocomplex nanocomposites. The results can be one of the guidelines for the preparation of PLA-based nanocomposites in the future.

EXPERIMENTAL METHODS

FT-IR spectra were recorded on a PerkinElmer spectrum 2000 spectrometer at a resolution of 1 cm^{-1}. ^1H NMR spectra were recorded on a Bruker Ultrashield 600 MHz/54 mm NMR spectrometer at room temperature using $CDCl_3$ as the solvent. The DSC analysis for all of the samples was performed on TA Instrument Q100 under N_2, following the method: equilibrate at 25 °C; ramp 10 °C/min to 250 °C; isothermal for 5 min; ramp 10 °C/min to 25 °C; isothermal for 5 min; ramp X °C/min to 250 °C (X is 3, 5, 7, and 10). WAXD diffractograms were obtained on a Bruker AXS D8 Advance thin film XRD instrument operating under a voltage of 40 kV and a current of 40 mA using Cu Kα radiation (λ=0.15418 nm). PLLA (3051D, M_n = 130K) pellets were purchased from Natureworks. Neat linear PDLA (M_n = 12 000) was purchased from Polymer Source. D-Lactide was purchased from PURAC Biochem. 1,4-Butanediol (BD) (ReagentPlus, 99%), 4-dimethylaminopyridine (DMAP), and tin(II) 2-ethylhexanoate (95%, $Sn(Oct)_2$) were purchased from Sigma Aldrich. *N*,*N*′-Dicyclohexylcarbodiimide (DCC) was purchased from Fluka. Other chemicals were used as received.

The synthesis of GO-g-PDLA occurred as follows. As the OH groups on GO could not be efficiently used as the initiator in the ring-opening polymerization of PDLA, more effective OH groups were attached by grafting BD onto COOH groups of GO under the catalysis of DCC and DMAP in DMF at room temperature overnight, followed by centrifuge wash for three times and overnight vacuum drying to obtain GO-BD. Recrystallized D-lactide monomer (4 g), GO-BD (20 mg, as initiators), $Sn(Oct)_2$ (35 μL, as catalyst), and anhydrous toluene (~50 mL) were charged into a round-bottom flask, and the flask was sealed, all done in a glovebox. A homogeneous mixture was obtained by ultrasonic for 20 min and then stirred at 120 °C for 3 days under reflux using a condenser in N_2. At the end of the reaction, the flask was cooled down to room temperature. At the flask bottom a sticky layer (GO-g-PDLA) was observed, which was separated from the rest of the solution and collected by dissolving in chloroform (200 mL), precipitating in excessive hexane (400 mL) and filtered by washing with methanol several times.

Stereocomplex nanocomposite preparation proceeded as follows. GO-g-PDLA and commercial PLLA were separately dissolved in chloroform. The resulting solutions were mixed together and casted to form nanocomposite films with different GO-g-PDLA contents denoted as X%-GO-D, where X stands for the GO-g-PDLA content, that is, 20 wt %, 10 wt %, and 5 wt %. Control samples denoted as X %-D were prepared accordingly using commercial neat linear PDLA. Neat PLLA films were prepared likewise without adding any PDLA species. Cold crystallized samples, including those of the stereocomplex nanocomposites and control samples, were obtained using DSC. The solution casting sample was sealed in the DSC aluminum pan and underwent the same thermal process as in the DSC experiments described above, except that the second heating scan was replaced by a ramp at 10 °C/min to 160 °C (a point between cold crystallization and melting), remaining isothermal for 5 min, and then quenching at 20 °C/min to room temperature.

AUTHOR INFORMATION

Corresponding Author

*E-mail: msehc@nus.edu.sg or cb-he@imre.a-star.edu.sg.

Notes

The authors declare no competing financial interest.

ACKNOWLEDGMENTS

The authors acknowledge the support from National University of Singapore for financial support (R-284-000-084-133) and provision of a scholarship for Sun Yang and Institute of Materials Research and Engineering (IMRE), under the Agency of Science, Technology, and Research (A*STAR) for materials analysis.

REFERENCES

(1) Tsuji, H.; Yamamoto, S.; Okumura, A. *J. Appl. Polym. Sci.* **2011**, *122* (1), 321−333.
(2) Tsuji, H. *Macromol. Biosci.* **2005**, *5* (7), 569−597.
(3) Woo, E. M.; Chang, L. *Polymer* **2011**, *52* (26), 6080−6089.
(4) Narita, J.; Katagiri, M.; Tsuji, H. *Macromol. Mater. Eng.* **2011**, *296* (10), 887−893.
(5) Xu, H.; Tang, S.; Chen, J.; Yin, P.; Pu, W.; Lu, Y. *Polym. Bull.* **2011**, 1−17.
(6) Lin, T. T.; Liu, X. Y.; He, C. *Polymer* **2010**, *51* (12), 2779−2785.
(7) Park, S.; Ruoff, R. S. *Nat. Nanotechnol.* **2009**, *4* (4), 217−224.
(8) Ramanathan, T.; Abdala, A. A.; Stankovich, S.; Dikin, D. A.; Herrera-Alonso, M.; Piner, R. D.; Adamson, D. H.; Schniepp, H. C.; Chen, X.; Ruoff, R. S.; Nguyen, S. T.; Aksay, I. A.; Prud'Homme, R. K.; Brinson, L. C. *Nat. Nanotechnol.* **2008**, *3* (6), 327−331.
(9) Lee, Y. R.; Raghu, A. V.; Jeong, H. M.; Kim, B. K. *Macromol. Chem. Phys.* **2009**, *210* (15), 1247−1254.
(10) Xu, Y.; Wang, Y.; Liang, J.; Huang, Y.; Ma, Y.; Wan, X.; Chen, Y. *Nano Res.* **2009**, *2* (4), 343−348.

(11) Verdejo, R.; Barroso-Bujans, F.; Rodriguez-Perez, M. A.; De Saja, J. A.; Lopez-Manchado, M. A. *J. Mater. Chem.* **2008**, *18* (19), 2221−2226.
(12) Dreyer, D. R.; Park, S.; Bielawski, C. W.; Ruoff, R. S. *Chem. Soc. Rev.* **2010**, *39* (1), 228−240.
(13) Xu, J. Z.; Chen, T.; Yang, C. L.; Li, Z. M.; Mao, Y. M.; Zeng, B. Q.; Hsiao, B. S. *Macromolecules* **2010**, *43* (11), 5000−5008.
(14) Murariu, M.; Dechief, A. L.; Bonnaud, L.; Paint, Y.; Gallos, A.; Fontaine, G.; Bourbigot, S.; Dubois, P. *Polym. Degrad. Stab.* **2010**, *95* (5), 889−900.
(15) Cao, Y.; Feng, J.; Wu, P. *Carbon* **2010**, *48* (13), 3834−3839.
(16) Wang, H.; Qiu, Z. *Thermochim. Acta* **2012**, *527*, 40−46.
(17) Wang, H.; Qiu, Z. *Thermochim. Acta* **2011**, *526* (1−2), 229−236.
(18) Pham, T. A.; Kumar, N. A.; Jeong, Y. T. *Synth. Met.* **2010**, *160* (17−18), 2028−2036.
(19) Hua, L.; Kai, W. H.; Yang, J. J.; Inoue, Y. *Polym. Degrad. Stab.* **2010**, *95* (12), 2619−2627.
(20) Zhang, J.; Tashiro, K.; Tsuji, H.; Domb, A. J. *Macromolecules* **2007**, *40* (4), 1049−1054.
(21) Zhang, J.; Sato, H.; Tsuji, H.; Noda, I.; Ozaki, Y. *J. Mol. Struct.* **2005**, *735*−*736*, 249−257.